

VĚDECKÉ SPISY VYSOKÉHO UČENÍ TECHNICKÉHO V BRNĚ

Edice PhD Thesis, sv. 455

ISSN 1213-4198

thesis
!
IS

Ing. Ivo Konvalina

**Quantification of Detection Efficiency
of the Detector of Secondary
Electrons in SEM**

BRNO UNIVERSITY OF TECHNOLOGY
FACULTY OF MECHANICAL ENGINEERING
INSTITUTE OF PHYSICAL ENGINEERING

ING. IVO KONVALINA

**QUANTIFICATION OF DETECTION EFFICIENCY OF THE
DETECTOR OF SECONDARY ELECTRONS IN SEM**

**KVANTIFIKACE DETEKČNÍ ÚČINNOSTI DETEKTORU
SEKUNDÁRNÍCH ELEKTRONŮ V REM**

SHORT VERSION OF PH.D. THESIS

Study field: Physical and Materials Engineering
Supervisor: Ing. Iona Müllerová, DrSc.
Opponents: Prof. Ing. Armin Delong, DrSc. (ISI ASCR, v.v.i., Brno)
Mgr. Karel Jurek, CSc. (IP ASCR, v.v.i., Praha)
Mgr. Marek Unčovský, Ph.D. (FEI CR, Ltd, Brno)
Presentation date: 13. 3. 2008

Keywords

collection efficiency, ET detector, detector of secondary electrons, electrostatic field, magnetic field, simulation of trajectories

Klíčová slova

sběrová účinnost, ET detektor, detektor sekundárních elektronů, elektrostatické pole, magnetické pole, simulace trajektorií

Disertační práce je uložena na oddělení vědy a výzkumu, VUT v Brně, FSI, Technická 2, 616 69 Brno.

CONTENTS

1 INTRODUCTION	5
2 STATE OF ART	6
2.1 DETECTOR OF SECONDARY ELECTRONS	6
2.2 COMPONENTS OF THE EVERHART-THORNLEY DETECTOR	7
2.3 COLLECTION EFFICIENCY	8
3 AIMS OF THE DISERTATION	9
4 QUANTIFICATION OF DETECTION EFFICIENCY OF THE DETECTOR OF SECONDARY ELECTRONS IN SEM	9
4.1 SOFTWARE AND METHODS	9
4.1.1 <i>SIMION 3D VERSION 7.0</i>	10
4.1.2 <i>MAGNETIC LENS DESIGN (MLD) & MAGNETIC LENS PROPERTIES (MLP)</i>	10
4.1.3 <i>WMUMI</i>	10
4.1.4 <i>STATISTIC METHOD FOR OBJECTIVE QUANTIFICATION OF DETECTION EFFICIENCY OF ET DETECTOR OF SECONDARY ELECTRONS</i>	11
4.1.5 <i>DEFINITION OF COLLECTION EFFICIENCY</i>	11
4.2 ET DETECTOR	13
4.2.1 <i>STAGE GEOMETRY</i>	14
4.2.2 <i>EMISSION ENERGY OF SECONDARY ELECTRONS</i>	16
4.2.3 <i>POTENTIALS OF GRID AND SCINTILLATOR</i>	17
4.2.4 <i>MAGNETIC FIELD OF OBJECTIVE LENS</i>	20
4.2.5 <i>AN OPTIMIZED SET-UP FOR A COMPLETE SPECIMEN CHAMBER</i>	23
4.3 DISCUSION OF RESULTS	24
5 CONCLUSION	26
6 REFERENCES	27

1 INTRODUCTION

Scanning Electron Microscopy (SEM) can image and analyse bulk specimens. In general, SEM is a vacuum system containing the electron source, focus optics and a detector. Electrons from a thermionic-, Schottky-, or field-emission cathode are accelerated by a voltage difference between cathode and anode that may be within the range 0.1 – 50 keV. The electron probe of diameter 100 nm – 1 nm, carrying the electron-probe current of 10 nA – 1 pA, is formed at the specimen surface. The deflection coil system scans the electron probe in a raster across the specimen synchronously with the observation screen, where its intensity is modulated by detected signal from the specimen. The diameter of the electron probe determines the geometrical resolution of SEM.

The focused electron beam impacts the specimen and interacts with its atoms. Elastic and inelastic scattering are the elementary atomic interaction processes, but the final signal is not the result of the single scattering process but of complete electron diffusion connected with gradual loss of the electron energy and lateral spreading caused by multiple elastic large-angle scattering. The electrons have a finite range R of the order of 10 nm – 10 μm , in dependence on electron energy and target density. The information and interaction volumes are not strictly limited and in most cases contribution to the signal decreases exponentially with increasing depth. The electrons that escape from the sample are called signal electrons and we can divide them into three basic parts: secondary electrons (SE), backscattered electrons (BSE) and Auger electrons (AE). The energy spectrum of the signal electrons is within the range from zero up to the primary beam energy. Furthermore, X-ray emission and cathodoluminescence can also be excited from the specimen.

Final image contrast depends not only on electron interaction with the specimen, but also on the part of the emitted electrons detected. The knowledge of the angular and energy sensitivity of the detector allows for a better interpretation of the final image contrast.

Detected signals in the SEM are mostly weak, therefore it is necessary to obtain the most effective conversion of electrons to the electrical signal that modulates brightness to achieve the highest possible signal to noise ratio (SNR). Three fundamental factors are important for the final contrast formation:

- Electron interaction with matter
- Collection efficiency of the detector
- Conversion of signal electrons to the electrical signal

The primary aim of this work is to study parameters affecting the collection efficiency (CE) of the detector of SE.

The topic of this dissertation is part of the long term program of the examination of the contrast and the detection in SEM, that is being solved by FEI Company in the cooperation with the Institute of Scientific Instruments AS CR, Brno.

A brief state-of-the-art knowledge of the detector of secondary electrons in the scanning electron microscope which is published in the technical literature, journals and proceedings of microscope conferences is introduced.

An outline of the aims that were specified before the beginning of the thesis is presented in Chapter 3.

Chapter 4 represents the core of the thesis. The method used for simulations and calculations of the collection efficiency of secondary electron detectors is described and CE is calculated for many different parameters and modifications of ET detector and arrangements of the specimen chamber. The standard ET detector below objective lens and also an in-lens SE detector and multi-channel detector are studied and presented.

A static method for objective quantification of the detector efficiency of the ET detector of secondary electrons is used for verification of results.

2 STATE OF ART

2.1 DETECTOR OF SECONDARY ELECTRONS

The oldest type of secondary electron detector is the Everhart-Thornley detector [1]. The detector is positioned on one side of the specimen chamber between the objective lens and the specimen. The electrostatic field of the detector penetrates to the specimen region and the emitted secondary electrons are attracted to the detector. Only a weak magnetic field of the objective lens exists at the specimen in this case.

A relatively new detection system is called in-lens detector, where the ET detector is placed in the objective lens. This detector is used in SEMs with the objective lens that produces strong magnetic field in the specimen region, from where secondary electrons are carried out into the objective lens by this magnetic field.

Each of these presented detector systems (see Figure 2.1.1) has different collection efficiency with its energy and angular sensitivity, as well as signal processing. Therefore different final contrast of the image can be expected in the different detection systems.

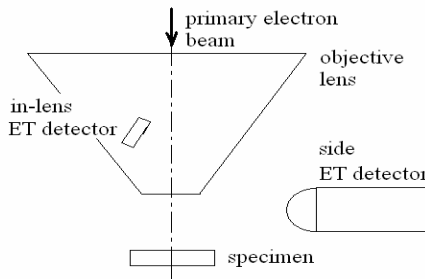


Figure 2.1.1. Basic types of the secondary electron detectors

2.2 COMPONENTS OF THE EVERHART-THORNLEY DETECTOR

The original design of the Everhart and Thornley detector (1960) [1] is shown in Figure 2.2.1. The secondary electrons leaving the specimen are collected, amplified and used to control the brightness of a cathode-ray tube scanned in synchronism with the primary electron beam. The detector consists of a cylindrical brass shield closed at the end facing the specimen by a grid cooper gauze and biased positively in order to attract the low-energy secondary electrons. Once through the grid, the electrons are accelerated toward the hemisphere of a plastic scintillator, the surface of which is covered with a 70 nm layer of aluminium. The intense electrostatic field, shaped by the focusing electrode, causes most electrons to strike the hemisphere near its apex. The light generated in the scintillator is guided by a Perspex light pipe to a commercial photomultiplier tube which then converts the light back to an electron signal and provides most of the required amplification.

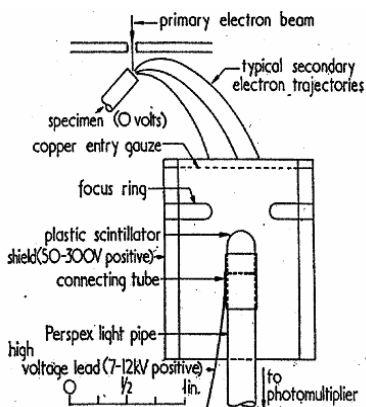


Figure 2.2.1 Everhart - Thornley detector (1960) [1]

At present, all SEMs are equipped by a similar type of ET detector, designed already in 1960, of course with various improvements and modifications.

Even though this work primarily deals with the simulations of the SE trajectories between the specimen region, the grid and the scintillator, and with the method of the detection quantum efficiency (DQE) measurement, let me shortly summarize the transfer of the signal through the whole detection channel. One of the most frequently used setups of the ET detector in a modern SEM is shown in Figure 2.2.2.

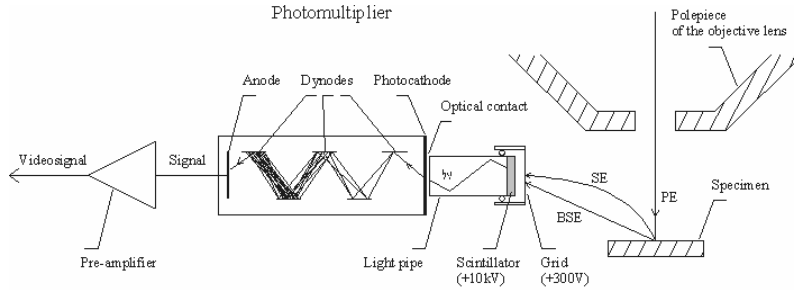


Figure 2.2.2 The ET detector arrangement

2.3 COLLECTION EFFICIENCY

The collection efficiency is defined as a portion of signal electrons that are hit by the detector from the ones emitted into the upper half-space.

But unfortunately, the same energy, current and impact angle of the primary beam and even one principle of the secondary electron detector still do not secure an identical image contrast. Magnetic and electrostatic fields in the specimen vicinity influence the secondary electrons trajectories, so that the collection efficiency of the detector and consequently the contrast of the image are strongly influenced.

As mentioned previously, the SEs are attracted to the ET detector by the positive grid bias, but some of them impact the wall and other parts in the specimen chamber. Some of BSEs also impact the scintillator, but the majority of them strike the wall, where the additional SEs and BSEs are generated that can reach the detector.

The distribution of the current in the chamber of the microscope is complicated and the detected signal is produced by several contributions, which can not be distinguished easily. Some kinds of signals can be eliminated by proper constructional arrangement of the detection systems. Oatley [2] measured currents in the microscope chamber. When the primary beam strikes the specimen, it produces both secondary electrons and high-energy backscattered electrons. Some of the BSE will go to the grid of the ET detector, while others will travel to the walls, where they will generate further SE and additional re-backscattered electrons which may travel to the grid, the specimen or to another part of the wall.

There are not a lot of published results dealing with collection efficiency of the SE detectors in SEM.

Bradley and Joy in 1991 [3] described a spreadsheet program for calculating secondary electron trajectories in electrostatic fields. They numerically solved the Laplace equation that sets the value of each point in the spreadsheet equal to the average of the values of the four points that surround it. The results of this calculation allow the equipotential lines and trajectories to be drawn.

The performance of a standard ET detector was analyzed by Balasubramanyam et al [4] in order to evaluate its efficiency when collecting SEs. The presented model

takes into account the contribution of all secondary electrons. The trajectories of SEs were simulated in 3D space between the specimen and the detector. The collection efficiency was calculated as a function of SE energy, the working distance and the grid potential. The optimum working distance for the greatest SE-I and SE-II collection is around 12 mm in the particular configuration studied.

Further works about this topic are not available in accessible literature.

3 AIMS OF THE DISERTATION

The aim of this work is analysis of some defined detection systems of the detectors of secondary electrons in SEM.

The core of the thesis is represented by simulations of the secondary electron trajectories in the specimen chamber of the microscope and studies of the factors influencing them. The detector of secondary electrons is a device consisting of several functional blocks. The knowledge of the detection characteristics of the detectors and their collection efficiency is very important for study of contrasts of the micrographs.

The aim is an analysis of the factors influencing the collection efficiency. It could not be studied earlier because suitable programs for 3D simulations of trajectories and also fast computing devices were not available. Only recently commercial programs have been developed that allow for study of the influence of electrostatic and magnetic fields, geometrical parameters of the detector and the complete microscope chamber on the secondary electron trajectories.

Several simulated and modified arrangements were verified by experiments. The study mainly focuses on the standard, side positioned ET detector of secondary electrons. Other parts deal with a study of the collection efficiency of the detectors in the scanning electron microscopy with slow primary beam electrons and multi-channel detectors in the cathode lens system.

4 QUANTIFICATION OF DETECTION EFFICIENCY OF THE DETECTOR OF SECONDARY ELECTRONS IN SEM

4.1 SOFTWARE AND METHODS

The SIMION 3D software, version 7.0 [5] is used for simulation of the collection efficiencies. Distributions of magnetic fields and aberrations of the objective lens are computed by programs Magnetic Lens Design (MLD) and Magnetic Lens Properties (MLP) [6]. Static parameters of the micrographs are calculated by WMUMI program [7].

The statistic method for objective quantification of the detection efficiency of the ET detector of secondary electrons was developed by the Institute of Scientific Instruments. The method is based on statistic processing of the output signal of the video channel, influenced by the detector quality. The collection efficiency of the detector is defined at the end of this chapter.

4.1.1 SIMION 3D version 7.0

SIMION 7.0 [5] is commercially available program that enables simulation of ion or electron optical problems with 2D, axially symmetrical and/or 3D, axially nonsymmetrical electrostatic and/or magnetic fields. A complex system or even the whole instruments can be simulated by this program. The geometry of the simulation systems, the potentials of electrodes and magnetic poles are defined in the workbench where the charged particles are flowing. The potentials in the points outside electrodes and poles are determined by solving the Laplace equation by finite difference methods.

4.1.2 Magnetic Lens Design (MLD) & Magnetic Lens Properties (MLP)

The MLD and MLP package is a set of programs for design and computation of the potential distribution of the axially symmetric magnetic lenses, and for computation of the optical electron properties of these fields [www.lencova.cz]. The finite element method is used in this programs [6].

4.1.3 WMUMI

WMUMI (Windows Matlab Unit for Microscope Imaging) is software for objective quantification of the static signal of the ET detector, written by L. Novák [8]. This software processes the final digital micrograph obtained from the output signal of the detection channel. An intensity X_i in each image pixel is a value from the assembly of the random quantity X .

The average value of a measured frame is

$$\langle X \rangle = \frac{1}{n} \sum_{i=1}^n X_i \quad (1)$$

and standard deviation

$$\sigma_n(X) = \left[\frac{1}{n-1} \sum_{i=1}^n X_i^2 - \frac{1}{n(n-1)} \left(\sum_{i=1}^n X_i \right)^2 \right]^{1/2} \quad (2)$$

Relative variation factor $V(X)$ characterizes quality of the final image

$$V(X) = \frac{\sigma(x)}{\langle X \rangle} \quad (3)$$

This quantity measures the quality of the checked micrograph. Good parameters of the detection channel, small noise in the signal, are characterized by the low value of the $V(X)$.

An alternative parameter that describes the detection channel is the signal to noise ratio

$$SNR = \frac{1}{V} \quad (4)$$

4.1.4 Statistic Method for Objective Quantification of Detection Efficiency of ET Detector of Secondary Electrons

The statistic method for objective quantification of the detection efficiency of the ET detector of SE is based on a statistical processing of the output signal of the videochannel described in the previous paragraph. The output signal is influenced by the detector quality; a stable input signal is required. The method compares SNR of the final digital images of the specimen free of any topographical and material contrast [9].

A suitable value of contrast for each arrangement was kept constant for the whole progress of the measurement. Very important is to adjust the brightness value that corresponds to the digital zero for no impact of the primary beam, because only under this condition you can use the full digital range of the AD converter. Channel adjustment was chosen for the working distance for which the intensity of the image was the highest. For each working distance the desired primary beam current was adjusted, the correct value was controlled by a picoammeter in a Faraday cage. The measured data were processed by the WMUMI software and the average value of image intensity, standard deviation and the relative variation factor were calculated.

The varying image intensity shows an effect of the working distance on the collection efficiency.

4.1.5 Definition of Collection Efficiency

The collection efficiency $C(E)$ for a particular emission energy E is calculated as a proportion of the SE trajectories, weighted by the cosine distribution of emission, that impact the detector from all trajectories emanating into the upper half-space:

$$C(E) = \frac{K_1}{2\pi} \int_{S_D} \cos \theta dS = \frac{K_1}{2\pi} \int_{\theta_{min}}^{\theta_{max}} \int_{-\varphi_x(\theta)}^{+\varphi_x(\theta)} \cos \theta \sin \theta d\varphi d\theta = \frac{K_1}{\pi} \int_{\theta_{min}}^{\theta_{max}} \varphi_x(\theta) \cos \theta \sin \theta d\theta \quad (5)$$

(see Figure 4.1.1 for definition of the quantities used in Eq. (5)).

Because $C(E) = 1$ for $\varphi_x(\theta) = \pi$, $\theta_{min} = 0$ and $\theta_{max} = \pi/2$, we get the constant as $K_1 = 2$. To keep the volume of simulation feasible, the trajectories were simulated for discrete values of θ chosen in 10° steps, while the limiting azimuthal angles for which the trajectory starts entering the detector were determined with the accuracy of 1° . The halved width of the angular interval between those limiting azimuthal angles appears in Eq. (5) as φ_x . The integral in Eq. (5) was then replaced with the integral sum

$$C(E) = \frac{2}{\pi} \sum_i \varphi_x(\theta_i) \cos \theta_i \sin \theta_i \Delta\theta \quad (6)$$

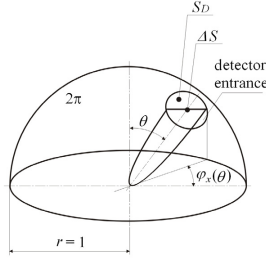


Figure 4.1.1 Definition of quantities appearing in Eqs. (5)

It is obvious that in order to obtain any realistic data comparable with those measured you have to take into account the full energy spectrum $N(E)$ of the SE emission, like the one shown in Figure 4.1.2.

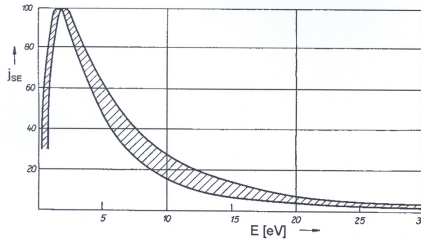


Figure 4.1.2 Range of energy spectra of secondary electrons measured for 10 different metals; data according to Kollath [10], reprinted from Hachenberg and Brauer [11]

To do this, the data obtained from Eq. (6) should be processed using the integral

$$C = \int_0^{\infty} C(E)N(E)dE = K \int_0^{\infty} C(E) \frac{EdE}{(E + \psi)^4} \quad (7)$$

where the expression for $N(E)$, derived by Chung and Everhart [12] as an approximate relation for the SE emission from conductive specimens, contains the work function ψ and the constant K . The work function chosen was 4.8 eV, which corresponds to carbon and also, for example, to Au. To normalize the results, we made the integral of the energy distribution $N(E)$ equal to 1 which, in turn, gives $K = 6\psi^2$. The integral in Eq. (7) was again approximated by the integral sum as outlined in Figure 4.1.3 [13].

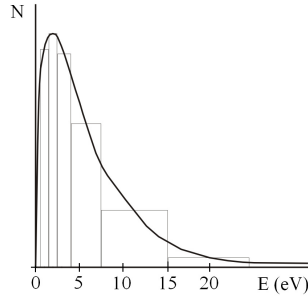


Figure 4.1.3 Integration over the energy spectrum of SE emission, approximated by six-term integral sum with variable steps

Using the procedure described above we arrived at the final results of this series of collection efficiency simulations, which reflects the energy distribution of SE and, hence, can approximate the true collection efficiency as it is measured by comparing the number of emitted and detected species. However, solely the SE-I signal is incorporated.

Simulations of the trajectories and calculations of the collection efficiency for several detectors of secondary electrons form the main part of this work. Properties of the collection systems of the detectors, e.g. standard ET detector, in-lens detector, multi-channel detector, in different scanning electron microscope systems are studied.

4.2 ET DETECTOR

The first task of this work was to evaluate the collection efficiency of the Everhart-Thornley detector of SE and to reveal fundamental rules for tailoring the set-ups in which efficient signal acquisition can be expected [14].

The cross section of the basic arrangement used in simulations, with the true shapes and relative dimensions of the objective lens and ET detector, is shown in Figure 4.2.1.

The working distance (w_d), the diameter of the specimen (d_{sp}), and the potential on the grid (U_g) were the main parameters varied in the individual simulation subtasks. It is supposed that the spatial distribution of the ground potential in the specimen vicinity influences the SE trajectories, so not only the specimen and pole-piece of the objective lens, but also the complete specimen stage are incorporated (see Figure 4.2.2 for the geometry of the specimen stage). The entire specimen chamber and its components at the ground potential were also taken into account.

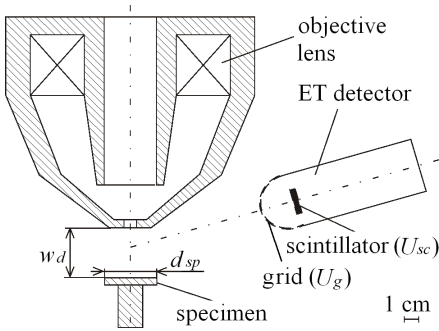


Figure 4.2.1 General cross section of the arrangement used in simulations. U_{sc} and U_g are positive potentials on the scintillator and grid, w_d is the working distance, and d_{sp} is the specimen diameter

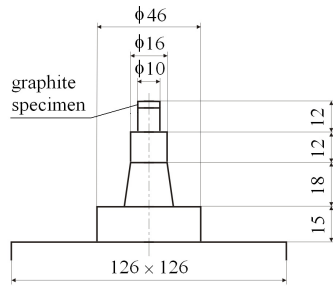
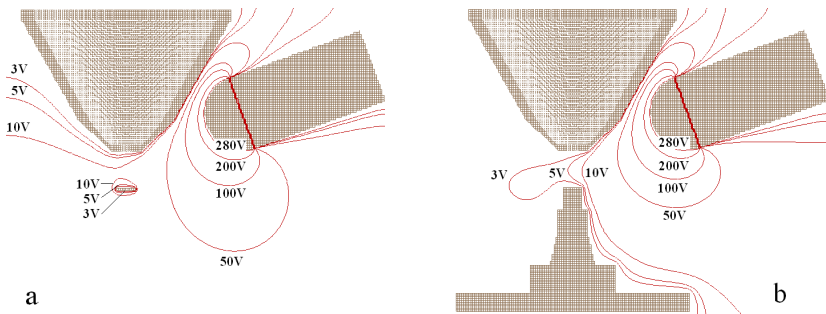


Figure 4.2.2 Cross section of the specimen stage

4.2.1 Stage Geometry

The simulation showed (Konvalina et al. 2004) [15] the existence of a big difference between collection efficiencies calculated for the arrangement of Figure 4.2.1 and for the same set-up but with the complete specimen stage as given in Figure 4.2.2. The distribution of the equipotentials calculated for both geometries is shown in Figure 4.2.3a and b, respectively, while the collection efficiencies are plotted in Figure 4.2.3c for an initial energy of the SE of 5 eV. All parts are at the ground potential, except the hemispherical grid, which is simulated with an equally shaped fixed equipotential at $U_g = +300$ V. In both simulation charts the specimen diameter is 10 mm and the $w_d = 20$ mm.



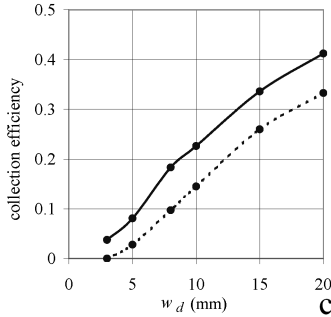


Figure 4.2.3 (a) and (b): Simulated equipotential surfaces for set-ups given in Figure 4.2.1 and 4.2.2, respectively. (c) Plots of collection efficiencies calculated for both arrangements. The dashed line holds for Figure 4.2.3a and the full line for Figure 4.2.3b. All parts are at the ground potential except for the hemispheric grid on which a potential of +300 V is applied. The diameter of the specimen is $d_{sp} = 10$ mm and working distance $w_d = 20$ mm. The collection efficiencies were calculated for the SE emission energy of 5 eV

Figure 4.2.3a shows a rather unrealistic set-up, and in comparison with Figure 4.2.3b reveals the main differences that concern the shapes of low potential iso-surfaces. The great volume of the matter at the ground potential like the real specimen stage, hinders penetration of the electrostatic field to the specimen vicinity, in particular to between the specimen and the pole-piece of the objective lens. When representing the specimen with a mere thin disc unsupported and levitating in free space, the extracting bias of the detector front grid forms a set of equipotential surfaces around the specimen so that the emitted electrons are not only accelerated to the half-space above the specimen or even toward the detector. This leads to the knowledge that one important feature of correct geometry is only moderate penetration of the grid field to above the specimen, which keeps the field vector pointing toward the detector. Figure 4.2.3c demonstrates significant differences in the collection efficiency caused by merely adding an appropriate stud and the rest of the grounded support to the specimen.

We also studied the influence of the specimen diameter on the collection efficiency – some preliminary data have been given by Konvalina and Müllerová (2003) [16]. As shown by Figure 4.2.4, the specimen diameter has no definite impact on the CE. At small working distances, the CE is a bit higher for larger specimen diameters, while the opposite holds when the w_d increases to >10 mm. However, these differences are not significant and do not require detailed interpretation.

These first simulations resulted in CE values significantly <1.0 in accordance with the predictions of the other authors cited above. Particularly at small w_d usual in the high-resolution mode of the SEM, the CE does not exceed 10 %, while even at unrealistically long w_d it still remains <0.5 [16,17].

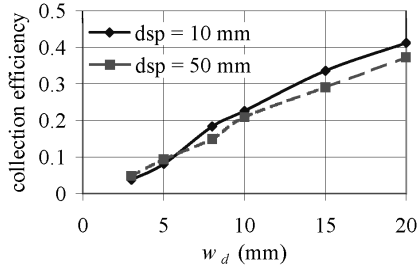


Figure 4.2.4 Calculated collection efficiency as a function of the w_d for two specimen diameters d_{sp} and secondary emission energy of 5 eV when the specimen holder according to Figure 4.2.2 is incorporated

4.2.2 Emission Energy of Secondary Electrons

To approximate the reality as much as possible we introduced at least some approximate energy distribution of the emitted SE as a source for the signal collection process. Quite naturally, this step has multiplied the overall number of the necessary simulations, in our case by the factor of 6 as the number of terms in the still very sparse sum approximating integration over the spectrum.

Simulated CEs for six discrete values of the initial SE energy are shown in Figure 4.2.5. You can see that at the shortest working distance the CE is very low. With increasing w_d the CE values start to differ according to the SE energy, and it is no surprise that the lowest initial energy of 1 eV is that for which the collection is most efficient at high working distances; however, even here the 30 % level is not exceeded. For a larger specimen diameter ($d_{sp} = 50$ mm) the results are very similar, but for the smallest working distances the CE is about 0.05 higher than what is obtained with a small diameter of the specimen. All simulations were performed for the specimen stage given in Figure 4.2.2 and for a hemispherical equipotential representing the grid at +300 V.

Figure 4.2.5 also compares the calculated collection efficiency as a function of the working distance for a fixed SE energy of 5 eV and for the full energy spectrum according to Eq. (7). The very small difference between the curves indicates that the complete energy spectrum of SE emission can be successfully represented by single emission energy and that 5 eV is a suitable choice. However, let me note that justification of this simplifying assumption has to be occasionally verified – our previous calculations have shown that when replacing the full energy spectrum with a fixed 5 eV value, you obtain (for the set-up given in Figure 4.2.1, that is, without the complete specimen holder and stage) the CE changing from 0.020 to 0.016 for a working distance of 5 mm and from 0.28 to 0.30 for $w_d = 20$ mm [18].

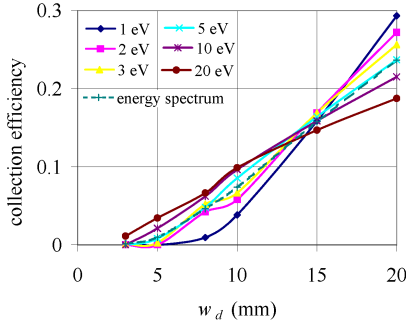


Figure 4.2.5 Calculated collection efficiency as a function of the w_d for several discrete energies of emitted electrons, when the specimen holder according to Figure 4.2.2 is considered. The dashed line is for the complete energy spectrum calculated according to Eq. (7). The grid potential is +300 V, set-up of Figure 4.2.1 and 4.2.2, specimen diameter $d_{sp} = 10$ mm, $U_{sc} = 10$ kV

4.2.3 Potentials of Grid and Scintillator

Further parameters affecting the simulation results are the front grid bias U_g and the scintillator potential U_{sc} .

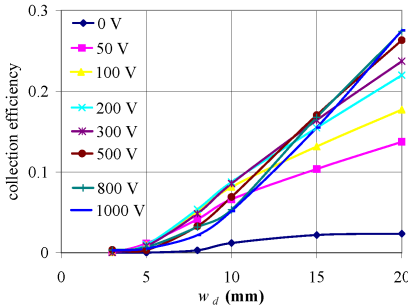


Figure 4.2.6 Calculated collection efficiency as a function of the w_d for several values of the front grid potential; specimen holder according to Figure 4.2.2, specimen diameter 10 mm, $U_{sc} = 10$ kV

The simplest approach was to replace the collector grid with a smooth equipotential of the same shape. The results are shown in Figure 4.2.6, again for the emission energy of 5 eV and the specimen diameter of $d_{sp} = 10$ mm. The magnitude of the front grid bias has showed itself to be surprisingly inconsequential, particularly at small working distances. Similar data have resulted from a larger specimen diameter ($d_{sp} = 50$ mm), again with some small increase in CE (of about

0.05) at the shortest working distances [19]. Naturally, the penetration of the increasing extraction field towards the specimen vicinity, and hence the optical axis, endangers perfect alignment of microscopes by deflecting the primary beam, particularly at low beam energies [3]. The field penetration up to the optical axis can be quantitatively assessed from the equipotentials drawn in Figure 4.2.7.

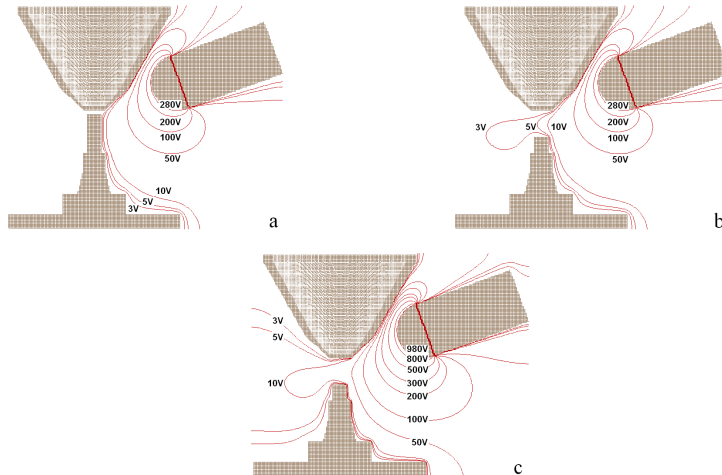


Figure 4.2.7 Simulated equipotentials showing field penetration from the biased grid toward the optical axis for the arrangement of Figure 4.2.1; specimen diameter $d_{sp} = 10$ mm; grid bias $U_g = +300$ V and working distance $w_d = 3$ mm (a); $U_g = +300$ V and $w_d = 20$ mm (b); $U_g = +1000$ V and $w_d = 20$ mm (c)

We often see formulations such as the front grid of the ET detector serving to attract SE toward the detector or the grid at the ground potential, and also to shield the high potential of the scintillator in order to prevent its impact on the trajectories of the primary beam electrons (Reimer 1998) [20]. As mentioned above, we started with the grid replaced by a smooth equipotential impenetrable for electrons, but a real grid is constituted of a net of wires allowing electrons to penetrate the equipotential and strike the scintillator. In this case, the potential distribution is more complicated (Read et al. 1999) [21] and again the particular transparency of such a system is below one. Another important circumstance is generation of SE directly on the grid wires under impact of the high energy backscattered electrons from the specimen or even the SE accelerated by the grid bias. These factors motivated us to omit the grid and to examine the field penetration from the scintillator towards the specimen region. In this connection we have also tested what influence is exerted by the position of the scintillator. The diameters of the scintillator and the working distance chosen were 20 mm and the scintillator was immersed in a grounded tube by 10 or 20 millimeters. The rough scale of the dimensions is apparent from the

drawing in Figure 4.2.1, and the calculated equipotentials are shown in Figure 4.2.8 for both cases.

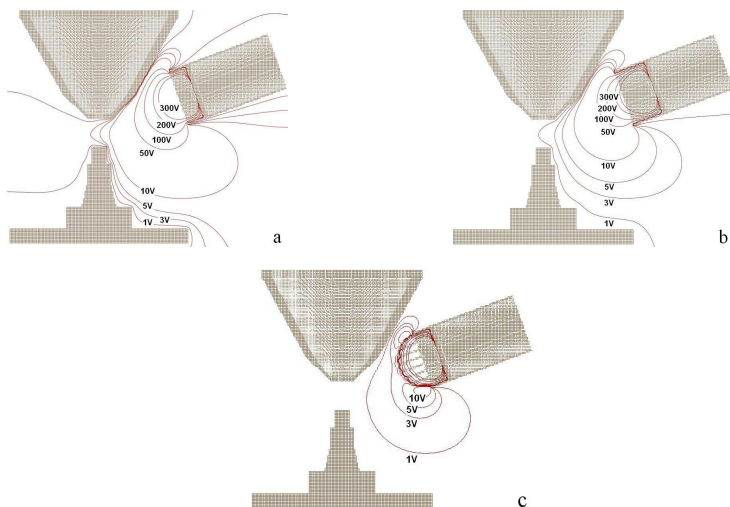


Figure 4.2.8 Simulated equipotentials around a scintillator 20 mm in diameter, held at +10 kV and immersed by 10 mm (a) or 20 mm (b) into a grounded tube. Field penetration from the scintillator at +10 kV through a grounded real grid (c); $w_d = 20$ mm, $d_{sp} = 10$ mm

The field configurations resulting from the various depths of immersion of the scintillator inside the tube indicate that an optimum exists for which the collection efficiency of the detector achieves its maximum, thereby utilizing the advantages of this grid-less system. The disadvantages include the problematic control of the collecting potential, which, for example, cannot be routinely optimized to a particular working distance when this is being varied [22].

For completeness, Figure 4.2.8c also shows the field penetration from the scintillator through a grid held at the ground potential. In this case, the true grid version was taken into account, namely a hemispherical cup of 40 mm in diameter, made from wires of a 1 mm diameter arranged in a 5 mm pitch, so that there are 6 of them both vertical and horizontal. You can see that the scintillator bias is shielded quite successfully and therefore does not endanger the beam alignment, although some extraction ability of the detector is still preserved.

Finally, we simulated the SE trajectories in the space between the above-described real grid and the scintillator (Figure 4.2.9). It is clearly visible that SE, once collected and having passed the grid, is well focused at the scintillator centre. However, at shorter working distances, electrons leaving the specimen under small polar angles (yellow trajectories) do not reach the scintillator at all – see Figure 4.2.9c. These simulations made it evident that the decrease in the collection efficiency, primarily lowering the signal-to-noise ratio, is also accompanied by

significant changes in the angular acceptance of the detector, which in turn might seriously alter the contrast generated [23].

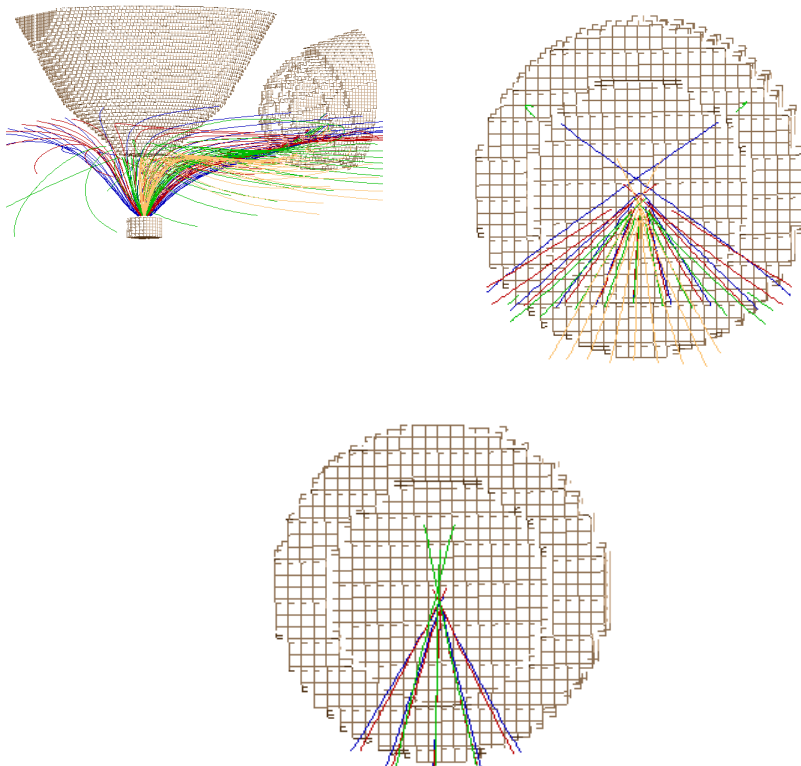


Figure 4.2.9 Three-dimensional imaging of secondary electron trajectories for $E_{SE} = 5$ eV, polar angle $\theta = 20^\circ, 40^\circ, 60^\circ,$ and 80° , full azimuthal angle $\varphi = 0^\circ$ to 360° with a step of 10° .

Real grid and scintillator are considered at potentials of $U_g = +300$ V and $U_{sc} = 10$ kV, respectively. Diameter of the specimen is $d_{sp} = 10$ mm. (a) Bundle of trajectories in the specimen chamber; (b, c) impact of SE on the scintillator for working distance 20 mm and 10 mm, respectively

4.2.4 Magnetic Field of Objective Lens

In all previous subtasks we did not assume any magnetic field penetrating from the objective lens (OL) towards the specimen vicinity. However, in general one has to consider this factor capable of affecting the SE trajectories. In the arrangement given in Figure 4.2.1, only a tiny influence of the magnetic field is expected as the field is closed between the OL pole-pieces. Hereinafter we will call this lens type the

"closed OL". To learn a bit more about SE trajectories leaving a specimen immersed in a stronger magnetic field, and at the same time to keep the geometry comparable with the previous geometry, we simply cut off the tip of the outer OL pole-piece. This OL type will be referred to as an "open OL" and is expected to deliver a rather strong magnetic field up to the specimen surface [24].

Cross-sections of both lenses and distributions of the magnetic field along the optical axis are shown in Figure 4.2.10. The programs MLD and MLP [6] were used for calculation of the axial magnetic field and aberration coefficients, respectively. The aberration coefficients and the maximum values of the axial field, together with its magnitudes at the specimen surface, are given in Table 4.2.1 for two working distances for both objective lenses in Figure 4.2.10. The OL excitation was taken as a constant for each lens, namely 505 Az for the closed OL and 1150 Az for the open OL. This implies the primary electron energy changing with the working distance of the specimen plane into which the primary beam is focused from infinity; for example, for the open OL the beam energies are 1206 eV at $w_d = 5$ mm and 10310 eV at $w_d = 20$ mm [25].

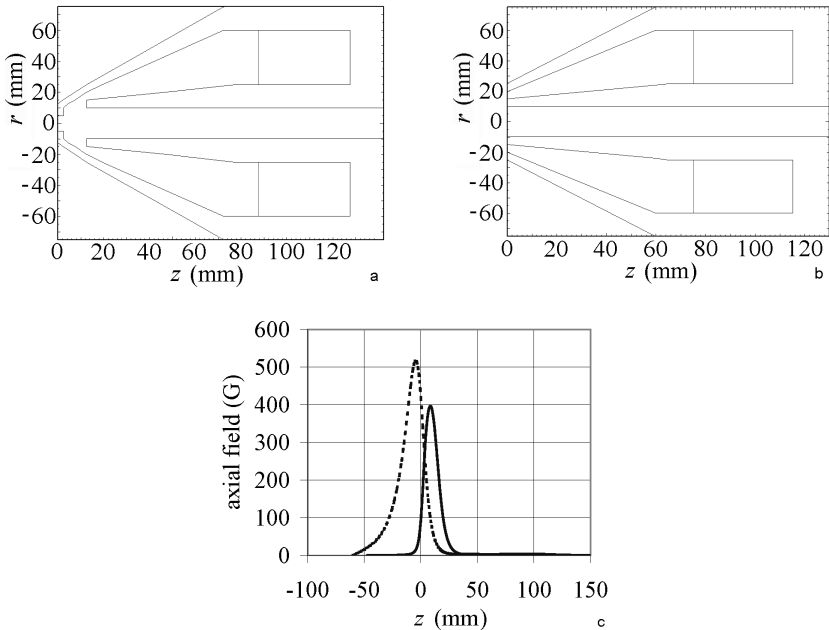


Figure 4.2.10 Cross section of the “closed OL” (a) and “open OL” (b), and distribution of the axial field for both lenses (c); full line for “closed OL”, dashed line for “open OL”

Table 4.2.1 The spherical (C_s) and chromatic (C_c) aberration coefficients, the maximum value of the axial magnetic field ($B^{axial\ max}$) and the magnetic field in the specimen plane $B^{axial\ spec}$ for imaging from infinity with both types of the OL shown in Figure 4.2.10

Objective lens	w_d (mm)	C_s (mm)	C_c (mm)	$B^{axial\ max}$ (G)	$B^{axial\ spec}$ (G)
Closed	20	191.76	27.11	396.91	1.23
Closed	5	27.42	12.60	591.25	19.12
Open	20	24.14	12.86	524.83	203.95
Open	5	2.79	3.96	1068.05	1067.76

Figure 4.2.11 shows the calculated CE for both OL types. Even for the "closed OL" it is evident that the CE improves a little when the influence of its moderate, outwards penetrating magnetic field is taken into account, especially at short working distances [15]. The strong magnetic field around the "open OL" collimates the SE trajectories towards the optical axis from the very beginning, thereby preventing the SE from reaching the side-attached detector in spite of any extraction electrostatic field applied.

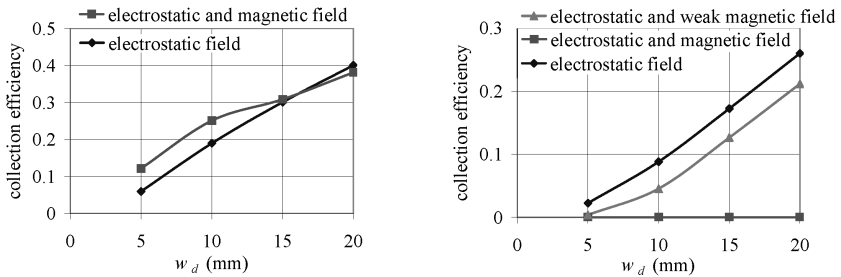


Figure 4.2.11 Comparison of the calculated CE between cases in which only the grid bias ($U_g = +300$ V) is applied, and when in addition the magnetic field of the OL is also taken into account. Simulations were conducted for "closed OL" (left) and "open OL" (right). The values of the axial magnetic field in the specimen plane are given in Table 4.2.2

Table 4.2.2 The axial magnetic field in the specimen plane for several working distances and for both types of OL with the "open OL" considered with "strong" and "weak" magnetic fields (see text). The OL excitation A corresponds to imaging from infinity to the specimen plane, excitation B secures a CE similar to the "closed OL"

Lens Type	OL excitation	w_d	5 [mm]	10 [mm]	15 [mm]	20 [mm]
Closed OL	A	[G]	19.1	4.1	1.7	1.2
Open OL, strong field	A	[G]	1067.8	730	374	204
Open OL, week field	B	[G]	4.5	3.7	2.6	1.7

The final attempt consisted of intentional lowering the excitation of the "open OL" so much that the residual on-specimen field allowed for collection of a number of SE comparable with what resulted for the "closed OL". In this way it was possible to assess the effect of the differently shaped pole-pieces and, therefore, the magnetic flux lines as well. The corresponding CE curve is included in Figure 4.2.11, and Table 4.2.2 summarizes the values of the axial magnetic field in the specimen plane for various working distances. Although for longer working distances at least this weakened magnetic field remains slightly above that of the "closed OL" with respect to the excitation needed to focus the primary beam of a reasonable energy (see above), this lowering exceeds two orders of magnitude. So much under-excited lens is of no use even with the slowest electrons. We can see that here the magnetic field in no case increases the CE, as was the case with the "closed OL".

4.2.5 An Optimized Set-Up for a Complete Specimen Chamber

Plenty of different designs were simulated in the context of this thesis, generated by combinations of details of the ET detector, such as the front grid shape and position and the orientation of the entire detector in the specimen chamber, together with the surrounding 3D distribution of potentials as a real specimen chamber, including all accessories. Naturally, the criterion applied was to secure a CE as high as possible. However, the task depends on so many parameters that it has not been possible to investigate more than just a limited variety of a number of intuitively chosen set-ups.

We arrived at a relatively successful and hence "optimized" design as follows: in addition to the "core assembly", consisting of the specimen, its holder and the pole piece of the objective lens, all held at the ground potential, and the grid biased to $U_g = +300$ V, the simulation chart incorporated a complete surrounding (grounded) specimen chamber – let us call it the "full set-up". The CE calculated for this complete set-up is compared in Figure 4.2.12 with that obtained for the mere "core assembly". To certain surprise, the surrounding mass at the ground potential contributes positively to an increase in CE. Figure 4.2.13 demonstrates that in this case an increase in the grid potential does improve the CE even at short working distances, in contrast to the arrangement of Figure 4.2.1 (see Figure 4.2.6 for results). Of course, one had still to be careful about electrostatic field penetration to the optical axis.

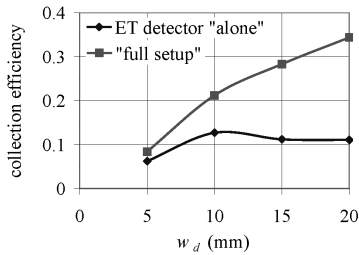


Figure 4.2.12 Calculated CE for the set-up in Figure 4.2.1 (the core assembly), when only the detector, specimen holder and pole-piece of the objective lens are considered in simulations (the ET detector "alone"), compared with the results obtained with the "full set-up" in which the entire specimen chamber at the ground potential is taken into account. The grid bias of the ET detector is $U_g = +300$ V, $U_{sc} = 10$ keV

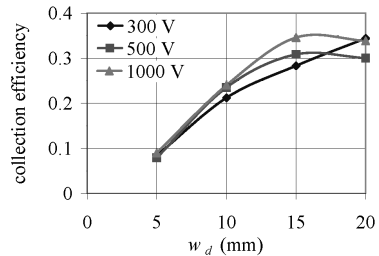


Figure 4.2.13 Calculated collection efficiency for the "full set-up" (entire specimen chamber) versus the working distance for various grid potentials

4.3 DISCUSION OF RESULTS

This work mainly deals with simulations of the trajectories of secondary electrons from the specimen to a side-positioned ET detector. The collection efficiency of this detector was calculated as a proportion of SE trajectories, weighted by the cosine distribution, that impact the active detector surface from all trajectories emitted into the upper half-space.

We studied the influences on the CE exerted by the specimen diameter, the shape of the specimen holder, the grid potential, the type and shape of the grid, the position of the detector, the magnetic field of the objective lens, and finally all grounded surfaces of the entire specimen chamber. The front, signal species attracting the grid was first replaced with a smooth equipotential of an identical shape, but later the real grid was introduced with the wires it is usually made of. In order to assess the impact on the focusing and alignment of the primary beam, the on-axis fields, both electrostatic and magnetic, were observed in every important case. Further a grid-less detector assembly (previously discussed by Reimer, 1998) [20] with the high-potential biased scintillator immersed in a grounded tube was examined. Electron trajectories between the grid and scintillator were also simulated – these results may be important for the conversion of electrons to photons (Atrata 1990) [26] as a process the efficiency of which is not constant over the scintillator surface (Schauer and Atrata 1992) [27].

We found it impossible to design an efficient ET detector only based upon a model arrangement incorporating the nearest neighborhood of the specimen-

detector join and, after inserting it into a real SEM, to expect any closer fit of the planned performance to the reality. The entire specimen chamber at the ground potential, the real geometry of the specimen holder and all other auxiliary parts (detectors, analyzers, guns, etc.) also had to be taken into account, as well as other electrostatic and magnetic fields, e.g. the field of the objective lens. For example, we found and documented that increase in the grid potential did not improve the CE, especially at low working distances, but this improvement was obtained if a particular complete chamber was introduced into the simulation chart.

At short working distances a weak magnetic field penetrating from the OL can improve the CE, while for longer w_d it is only the grid bias that is effective in improving the CE. With $U_g = 1000$ V, a CE of about 0.09 can be achieved for $w_d = 5$ mm, and as much as 0.34 for $w_d = 20$ mm (the grid as a transparent electrode was used in this simulation). In this case the potential on the optical axis was about 0.13 V for $w_d = 5$ mm, but as much as 2.2 V for $w_d = 20$ mm. An even better collection efficiency can be achieved if the ET detector is tipped over in such a way that its axis appears in the specimen plane ($\theta = 90^\circ$).

All our results indicate that it is very difficult, if not impossible, to have for this detector type a high CE at short working distances. It is simply due to their non-zero emission energies that SE do not follow the lines of force and, moreover, at short working distances these lines do not point exactly towards the detector but rather to the OL pole-piece. Modern SEMs usually have very efficient in-lens (or through-the-lens) detectors towards which nearly all SE are transported by tailored distributions of fields inside the OL bore. Another advantage is that the tertiary SE emitted from, for example, the OL pole-piece, do not reach detectors situated above OL. Instructive in this respect are the measured values of CE presented by Agemura et al. (2001) [28] who examined the geometrical collection efficiency for secondary electrons in the Hitachi S-4500 SEM as a function of the working distance. At the working distance of $w_d = 20$ mm they established CE = 0.32 for the "lower" side-attached SE detector, and CE = 0.5 for the "upper" in-lens detector. These measurements were performed for working distances from 5 to 30 mm, with the resulting CE between 0.8 and 0.24 for the in-lens detector and from nearly zero to 0.73 for the lower detector.

We might want to detect all SE emitted from the specimen and thereby achieve a high signal to noise ratio (S/N), but we have to realize that some image contrasts are not borne by local differences in the emission yields but in their angular distributions. We lose information when integrating these distributions via the total collection of signal species. First of all the topographical contrast can be nearly lost when all SEs are detected. If only part of the emitted electrons is acquired according to the azimuthal and polar angles of their trajectories, the S/N ratio decreases but the contrast increases. Contrast formation by means of in-lens and side-attached SE detectors was discussed, for example, by Cazaux [29].

Let us conclude that especially the topographical contrast in the secondary electron mode is strongly influenced by the collection efficiency and varies with all

the parameters of the microscope discussed above. The different appearance of micrographs of the same specimen acquired in different SEM devices can result from the uneven working distances, but more probably from uneven distributions of surrounding fields even at equal working distances. The real situation is further complicated by the ability of the detector to collect not only the true, primary electron excited SEs (Oatley 1983, Peters 1996, Reimer 1998) [2, 30, 20], and by the presence of local fields on the specimen, connected with charging, contamination, etc.

More-detailed discussions of the detection problems in SEM lead to a single conclusion, namely that the "correct" detection approach is to collect all emitted electrons but to do this by means of a multi-channel, two-dimensional position sensitive detector in such a way that the original emission angle is preserved. Above all, the possibility of sensing the emission energy appears the ultimate completion. Only then there is a chance that all generated information is really acquired.

5 CONCLUSION

The thesis "Quantification of Detection Efficiency of Detector of Secondary Electrons in SEM" is closely focused on the study of the detection characteristics, mainly on the collection efficiency of the detector, which radically influences the quality of the final micrograph. The signal electrons are emitted from the specimen after primary beam impact and are influenced by many factors. However, you cannot take control of all of them.

We suggested a method for calculation of the collection efficiency, which is based on several different programs. Application of the results of these programs allows us to study a particle move (trajectories) in various scanning electron microscopes where electrostatic and (or) magnetic fields are presented.

The calculated results of the collection efficiency show certain possibilities of optimization of some parts of the ET detector or other components in the specimen chamber. Chosen simulated arrangements were realized and experimentally verified. The measured collection efficiencies supported corrections of simulations, in particular as regards changes induced by various modifications.

The factors that influence collection efficiency of the ET detector were analyzed. The thesis describes both the influence of the electrostatic field of the detector and the magnetic field of the objective lens, whose measurement is given by the type and the parameters of the objective lens. Great efforts were put into study of the influences of the geometrical parameters (geometry of the individual parts of the ET detector and geometry of the other components in the specimen) that change the distribution of the electrostatic field.

Detection systems in the low energy scanning electron microscopes were simulated, too. In-lens secondary electron detector in the microscope with single-pole objective lens reaches great collection efficiency for small working distances and low primary beam energy.

6 REFERENCES

- [1] EVERHART, T.E., THORNLEY, R.F.M. Wideband detector for micro-micro-ampere low-energy electron currents. *Journal of Scientific Instruments*. 1960, vol 37, no. 7, p. 246-248.
- [2] OATLEY, C.W. Electron currents in the specimen chamber of a SEM. *Journal of Physics E-Scientific Instruments*. 1983, vol. 16, no. 4, p. 308-312. ISSN 0022-3735.
- [3] BRADLEY, G.L., JOY, D.C. Spreadsheet program for calculating secondary electron trajectories in electrostatic fields. In *Proceedings of the 49th Annual Meeting of the Electron Microscopy Society of America*. San Francisco (USA): San Francisco Press, 1991, p. 534-535.
- [4] BALASUBRAMANYAM, M., MUNRO, E., TAYLOR, J. Secondary electron detection in the scanning electron microscope. *Nuclear Instruments & Methods in Physics Research Section A-Accelerators Spectrometers Detectors and Associated Equipment*. 1995, vol. 363, no. 1-2, p. 270-275. ISSN 0168-9002.
- [5] DAHL, D.A. SIMION for the personal computer in reflection. *International Journal of Mass Spectrometry*. 2000, vol. 200, no. 1-3, p. 3-25. ISSN 1387-3806.
- [6] LENCOVÁ, B., WISSELINK, G. Program package for the computation of lenses and deflectors. *Nuclear Instruments & Methods in Physics Research Section A-Accelerators Spectrometers Detectors and Associated Equipment*. 1990, vol. 298, no. 1-3, p. 56-66. ISSN 0168-9002.
- [7] MÜLLEROVÁ, I. Report on the project: Optimization of the secondary electron detector, part one: Image processing software for the static method (program WMUMI), ÚPT AV ČR. 2004.
- [8] NOVÁK, L. Detekční účinnost Everhart-Thornleyho detektoru sekundárních elektronů v rastrovacím elektronovém mikroskopu. Diplomová práce. *MU Brno*. 2004.
- [9] FRANK, L., MÜLLEROVÁ, I., NOVÁK, L., HORÁČEK, M., KONVALINA, I. A method for objective quantification of the efficiency of electron detectors. In *EMC 2004 – Proceedings of the 13th European Microscopy Congress*. Antwerp, (Belgium): Belgian Society for Microscopy, 2004, p. 67-68.
- [10] KOLLATH, R. Sekundärelektronen-Emission fester Körper bei Bestrahlung mit Elektronen. *Handbuch der Physik 21* (ed. S. Flügge), Springer, Berlin, 1956. p. 232-306.
- [11] HACHENBERG, O., BRAUER, W. Secondary electron emission from solids. *Adv. electronics and electron physics*. 1959, vol. 11, p. 413-499.
- [12] CHUNG, M.S., EVERHART, T.E. Simple calculation of energy distribution of low-energy secondary electrons emitted from metals under electron bombardment. *Journal of Applied Physics*. 1974, vol. 45, no. 2, p. 707-709. ISSN 0021-8979.
- [13] KONVALINA, I. Kvantifikace detekční účinnosti detektoru sekundárních elektronů v REM. In *PDS 2003 - Sborník prací doktorandů prezentovaných na Seminári oddělení Elektronové optiky na počátku roku 2004*. Brno: Institute of Scientific Instruments AS CR, 2004, p. 31-38. ISBN 80-239-2268-8.
- [14] KONVALINA, I., MÜLLEROVÁ, I. The Trajectories of Secondary Electrons in the Scanning Electron Microscope. *Scanning*. 2006, vol. 28, no. 5, p. 245-256. ISSN 0161-0457.
- [15] KONVALINA, I., MÜLLEROVÁ, I., FRANK, L. Influence of magnetic and electrostatic fields in the specimen vicinity on trajectories of secondary electrons in SEM. *Autumn School on Materials Science and Electron Microscopy 2004 - Emerging Microscopy for Advanced Materials Development: Imaging and Spectroscopy on Atomic Scale*. Berlin (Germany), 2004, p. 24.
- [16] KONVALINA, I., MÜLLEROVÁ, I. Efficiency of collection of the secondary electrons in SEM. *Microscopy and Microanalysis*. 2003, vol. 9, supp. 3, p. 108-109. ISSN 1431-9276.
- [17] KONVALINA, I., MÜLLEROVÁ, I. Účinnost sběru sekundárních elektronů v REM. In *Mikroskopie 2004 – Přednášky*. 2004, p. 30.
- [18] KONVALINA, I. Kvantifikace detekční účinnosti detektoru sekundárních elektronů v REM. In *PDS 2006 – Sborník prací doktorandů oboru Elektronová optika*. Brno: Institute of Scientific Instruments AS CR, 2006, p. 25-28. ISBN 80-239-7957-4.
- [19] KONVALINA, I., MÜLLEROVÁ, I. Factors affecting the Collection Efficiency of Secondary Electrons in SEM. In *Proceedings of the 6th Dreiländertagung Microscopy Conference 2005*. Davos (Switzerland): Paul Scherrer Institute, 2005, p. 48. ISBN 1019-6447.

- [20] REIMER, L. Scanning Electron Microscopy – Physics of Image Formation and Microanalysis. *Berlin: Springer-Verlag*, 1998. 527 pages. ISBN 3-540-63976-4.
- [21] READ, F.H., BOWRING, N.J., BULLIVANT, P.D., WARD, R.R.A. Short- and long-range penetration of fields and potentials through meshes, grids or gauzes. *Nuclear Instruments & Methods in Physics Research Section A-Accelerators Spectrometers Detectors and Associated Equipment*. 1999, vol. 427, no. 1-2, p. 363-367. ISSN 0168-9002.
- [22] KONVALINA, I., MÜLLEROVÁ, I. Collection efficiency of the detector of secondary electrons in SEM. In *Proceedings of the 9th International Seminar Recent Trends in Charger Particle Optics and Surface Physics Instrumentation*. Skalský Dvůr: Institute of Scientific Instruments AS CR, 2004, p. 41-42. ISBN 80-239-3246-2.
- [23] KONVALINA, I., MÜLLEROVÁ, I. Sběrová účinnost ET detektoru sekundárních elektronů v REM. In *Mikroskopie 2005 – Přednášky*. 2005, p. 13.
- [24] KONVALINA, I., MÜLLEROVÁ, I., FRANK, L. The collection efficiency of the Everhart-Thornley detector of secondary electrons in SEM. In *EMC 2004 - Proceedings of the 13th European Microscopy Congress*. Antwerp, (Belgium): Belgian Society for Microscopy, 2004, p. 79-80.
- [25] KONVALINA, I. Kvantifikace detekční účinnosti detektoru sekundárních elektronů v REM. In *PDS 2004 - Sborník prací doktorandů prezentovaných na Semináři oddělení Elektronové optiky*. Brno: Institute of Scientific Instruments AS CR, 2005, p. 31-34. ISBN 80-239-4561-0.
- [26] AUTRATA, R. A modification of the ET secondary electron detector with a single crystal scintillator. *Scanning*. 1990, vol. 12, p. 119-125. ISSN 0161-0457.
- [27] SCHAUER, P., AUTRATA, R. Light transport in single-crystal scintillation detectors in SEM. *Scanning*. 1992, vol. 14, no. 6, p. 325-333. ISSN 0161-0457.
- [28] AGEMURA, T., FUKUHARA, S., TODOKORO, H. Measurement technique for the incident electron current in secondary electron detectors and its application in scanning electron microscopes. *Scanning*. 2001, vol. 23, no. 6, p. 403-409. ISSN 0161-0457.
- [29] CAZAUX, J. Recent developments and new strategies in scanning electron microscopy. *Journal of Microscopy – Oxford*. 2005, vol. 217, p. 16-35. ISSN 0022-2720.
- [30] PETERS, K.R. Collection deficiencies of scanning electron microscopy signal contrasts measured and corrected differential hysteresis image processing. *Scanning*. 1996, vol. 18, no. 8, p. 539-555. ISSN 0161-0457.

Curriculum Vitae

Name: Ivo KONVALINA

Born: March 23th 1979 in Brno

Contact: konvalina@isibrno.cz

Education

- 1997–2002 **Brno University of Technology / Faculty of Electrical Engineering and Communication Department of Microelectronics**
State exam passed in June 2002
Diploma thesis Gas Desorption under a Fall of Electrons defended in June 2002
- 2002–2008 **Brno University of Technology / Faculty of Mechanical Engineering Department of Physical Engineering**
Ph.D. study
State exam passed in October 2005

Experience

2002 – to date **Institute of Scientific Instruments AS CR v.v.i., Department of Electron Optics**

Languages

English

Participant on grants and projects

- 2006 – 2008 Detection system for the record of the pure secondary electrons or backscattered electrons signals in ESEM (GA AS CR - KJB200650602)
- 2005 – 2007 Direct imaging of the dopant distribution in a semiconductor by means of low energy electrons (GA CR - GA102/05/2327)
- 2005 – 2007 Detection of signal electrons in scanning electron microscopy with low primary beam energies (GA AS CR - KJB200650501)
- 2006 Project on the electron beam technology (FEI Company Eindhoven, The Netherlands)
- 2005 Development of detection methods for SEM (FEI Czech Republic, Ltd)
- 2005 – 2004 Optimization of the detector of secondary electrons (FEI Czech Republic, Ltd)
- 2003 Development of a method for objective quantification of the detection efficiency of the Everhart-Thornley detector of secondary electrons (FEI Czech Republic, Ltd)

Abstract

Three-dimensional simulations of the trajectories of secondary electrons in the scanning electron microscope have been performed for plenty of real configurations of the specimen chamber, including all its basic components. The primary purpose was to evaluate the collection efficiency of the Everhart-Thornley detector of secondary electrons and to reveal fundamental rules for tailoring the set-ups in which efficient signal acquisition can be expected. Intuitive realizations about the easiness of attracting the secondary electrons towards the biased front grid of the detector have shown themselves as likely false, and all grounded objects in the chamber have proved influencing the spatial distribution of the signal-extracting field. The role of the magnetic field penetrating from inside the objective lens is shown to play an ambiguous role as regards possible support for the signal collection.

Abstrakt

3D modelování trajektorii sekundárních elektronů v rastrovacím elektronovém mikroskopu bylo realizováno pro mnoho reálných konfigurací komory vzorku, včetně všech jejích základních komponent. Prvořadým záměrem bylo vyhodnotit sběrovou účinnost Everhartova-Thornleyho detektoru sekundárních elektronů a stanovit základní pravidla pro úpravu uspořádání pro dosažení účinné signálové akvizice. Intuitivní představy snadného přitažení sekundárních elektronů k síťce s kladným potenciálem se ukázaly chybné, všechny komponenty na zemním potenciálu v komoře prokazatelně ovlivňují prostorové rozložení extrakčních polí. Magnetické pole prosakující z vnitřku objektivové čočky, jak je ukázáno, hraje víceznačnou roli v možnosti podpory sběru signálu.